Short Communication

Effect of Heat Treatment and Passivation on Corrosion Behavior of Electroless Ni-P Coating on 20# Steel in Simulated Soil Solution

Guoyun Tong [1], Liying Yu[2,*]

[1] Hebei Vocational University of Industry and Technology, Shijiazhuang 050091, China;
[2] Hebei Polytechnic Institute, Shijiazhuang 050091, China
*E-mail: 100296@yzpc.edu.cn

Ni-P coating was prepared on 20# steel by electroless deposition. And then, the Ni-P coating was treated by heat treatment and passivation sequentially to greatly improve its corrosion resistance in simulated soil solution. The corrosion resistance was evaluated by potentiodynamic polarization curves and immersing testing. The results show that, the corrosion rate and corrosion current density of the Ni-P coating treated by heat treatment and passivation is 0.12 g/(cm^2·d) and 2.49×10^{-6} A/cm^2 respectively after immersing in simulated soil solution for 16 days, showing excellent corrosion resistance. However, the corrosion rate and corrosion current density of 20# steel is 1.73 g/(cm^2·d) and 2.06×10^{-4} A/cm^2 respectively after immersing in simulated soil solution for 16 days, indicating poor corrosion resistance. Ni-P coating itself has good corrosion resistance, and it presents excellent corrosion resistance after heat treatment and passivation, which is beneficial to protect 20# steel in simulated soil solution.

1. INTRODUCTION

20# steel is a kind of high quality carbon structural steel and its plasticity, toughness and welding performance is good, which is suitable for the manufacture of oil and gas transmission pipelines [1-5]. The oil or gas pipelines are usually buried in the ground with soils and are corroded by water, chlorine salts and sulfate for a long time. Especially, when buried in an alkaline soil environment containing a variety of salts, pipelines are prone to corrosion and the degree of corrosion is often more serious. Scholars engaged in related topics have found that pipelines present various corrosion forms such as pitting corrosion, uniform corrosion and crevice corrosion in soil, and surface

treatment is an effective measure to inhibit pipeline corrosion in soil [6-8].

At present, a metal protection coating is usually prepared on the surface of pipeline steel to improve its corrosion resistance. For example, Li et al. [9] used a kind of laser cladding process to prepare a Ni-Cr-Mo alloy coating on the surface of pipeline steel, and they found that Ni-Cr-Mo alloy coating has good comprehensive performance and can effectively inhibit corrosion of pipeline steel. Lin et al. [10] used the electroless deposition technology to prepare a Ni-P coating on the surface of P110 oil pipeline steel. The experimental results showed that Ni-P coating could significantly improve the corrosion resistance of P110 oil pipeline steel. Tian et al. [11] used a kind of double glow plasma process to prepare a G3 alloy-like coating on the surface of P110 oil pipeline steel. The corrosion resistance performance of P110 oil pipeline steel was significantly improved. Sherif et al. [12] adopted high velocity oxy-fuel deposition process to prepare two kinds of coating on the surface of API-2H pipeline steel to inhibit API-2H pipeline steel corrosion. Moreover, Wang et al. [13] also used the electroless deposition technology to prepare a Ni-P coating on the surface of API X100 pipeline steel, and they found that Ni-P coating was suitable for corrosion protection of pipeline steel.

However, compared with single surface treatment technology, using two or more kinds of surface treatment technology has many advantages which are expected to achieve a better effect. In this paper, 20# steel is selected as the research object, simulated soil solution is prepared as the corrosion medium, and the Ni-P coating is treated by heat treatment and passivation to improve its corrosion protection for 20# steel in simulated soil solution. The research topic is innovative, and the experimental results in this paper can provide references for scholars engaged in related research.

2. EXPERIMENTAL

2.1 Materials

The substrate is 20# steel sheet, and its chemical composition (mass fraction, %) is as follows: 0.17~0.24% C, 0.17~0.37% Si, 0.35~0.65% Mn, 0.035% P, 0.25% Cr, 0.25% Ni, and the rest is Fe. The substrate is cut into two different sizes: 30 mm×12 mm×2 mm and 12 mm×12 mm×2 mm. The former is used to test the corrosion rate and observe the corrosion morphology of samples after immersing in simulated soil solution for different days, and the latter is used for electrochemical corrosion testing.

2.2 Heat treatment and passivation of electroless Ni-P coating on 20# steel

2.2.1 Pretreatment of 20# steel

The 20# steel substrate is polished by different grades of sandpapers. After that, the substrate is immersed in an alkali solution (40 g/L NaOH and 10 g/L Na_2CO_3, 10 minutes, 65 °C) and an acid solution (15% HCl, 1 minute, room temperature) sequentially to clean the surface.

2.2.2 Electroless deposition of Ni-P coating on 20# steel

The chemical composition of the solution for electroless deposition of Ni-P coating is listed in Table 1. The pre-treated 20# steel is immersed in 200 ml electroless solution listed in Table 1 to prepare Ni-P coating. The pH value of the solution is adjusted to 10 using 1 mol/L sodium hydroxide solution. The electroless deposition lasts for 2 hours at 88 ℃. After the electroless Ni-P coating is finished, the sample is washed and dried.

Table 1. Chemical composition of the solution for electroless deposition of Ni-P coating; (all the chemical agents are analytically pure)

Chemical agents	Concentration
$NiSO_4 \cdot 6H_2O$	25 g/L
$NaPO_2H_2 \cdot H_2O$	32 g/L
$C_6H_8O_7 \cdot H_2O$	18 g/L
$C_3H_6O_3$	6 ml/L
$C_4H_6O_4$	3 g/L
Sodium dodecyl sulfate	0.06 g/L

2.2.3 Heat treatment of electroless Ni-P coating on 20# steel

The electroless Ni-P coating on 20# steel is placed in the muffle furnace at room temperature and heated to 400 ℃ by applying a heating rate of 5 ℃/min. The sample is kept for 1 hour at 400 ℃ and then is cooled calmly at room temperature. The heat treatment of electroless Ni-P coating is defined as HT Ni-P coating in the following.

2.2.4 Passivation of electroless Ni-P coating on 20# steel after heat treatment

After heat treatment, the sample is immersed in the passivation solution with 35 g/L $K_2Cr_2O_7$ for 10 minutes at 60 °C to carried out the passivation. The electroless Ni-P coating after heat treatment and passivation is defined as Ni-P coating after HT and PA in the following.

2.3 Performance testing

2.3.1 Corrosion rate testing

Weight loss method is used to test the corrosion rate of different samples after immersing in simulated soil solution for different time and the unit is $g/(cm^2 \cdot d)$. Table 2 lists the main composition of simulated soil solution, and the pH value is adjusted to 9.3~9.4 using 10% sulfuric acid or sodium hydroxide solution. In order to reduce the error and obtain a more accurate corrosion rate, the samples are weighed by precision electronic balance before and after the experiment, and the average value is

measured several times.

Table 2. Main composition of simulated soil solution; (all the chemical agents are analytically pure)

Chemical agents	NaCl	NaHCO$_3$	Na$_2$SO$_4$	CaCl$_2$	MgCl$_2$	KNO$_3$
Concentration/ (g·L^{-1})	3.17	0.15	2.50	0.26	0.70	1.24

2.3.2 Surface morphology characterization and corrosion products analysis

MERLIN Compact scanning electron microscopy (SEM) is used to characterize the surface morphology of different samples and the corrosion morphology after immersing in simulated soil solution for different time. A local area of the sample is selected and amplified by 10000 times in the autofocus mode. In addition, the corrosion products generated on the surface of different samples are analyzed by energy spectrometer with working voltage 20 kV.

2.3.3 Electrochemical testing

Parstat2273 electrochemical workstation is used to test the potentiodynamic polarization curves of different samples immersing in simulated soil solution for different time. The saturated calomel electrode, platinum sheet and different samples are used as reference electrode, auxiliary electrode and working electrodes, respectively. The scan rate is 1 mV/s, and the corrosion potential and corrosion current density are obtained from the results of polarization curve testing, which are used to evaluate the corrosion resistance of different samples in simulated soil solution.
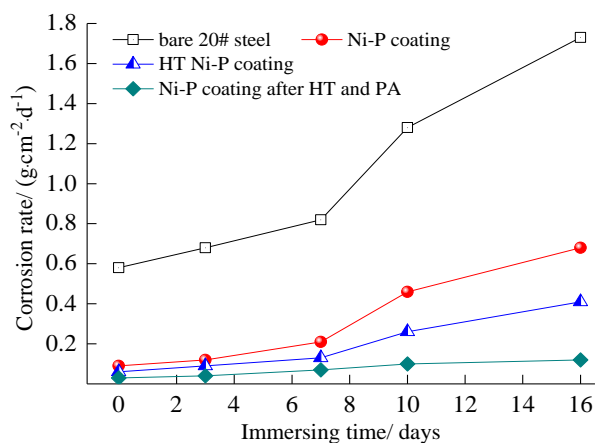
3. RESULTS AND DISCUSSION

3.1 Corrosion rate analysis

Figure 1 shows the corrosion rate of different samples after immersing in simulated soil solution for different time. As shown in Figure 1, the corrosion rate of 20# steel increases slowly at the early stage of immersing in simulated soil solution. The reason is that with the extension of immersing time, a dense corrosion products layer is gradually formed on the surface of 20# steel, which can prevent corrosive ions and delay the development of corrosion. However, the corrosion rate of 20# steel increases significantly to 1.73 g/(cm^2·d) at the later stage of immersing in simulated soil solution, indicating a serious corrosion degree. The reason is that the corrosion products layer generated on the surface of 20# steel after immersing for longer time will crack due to dehydration, and the corrosive ions will spread along the cracks to further aggravate the corrosion degree of 20# steel. The corrosion rate of Ni-P coating and HT Ni-P coating in simulated soil solution is similar to that of 20# steel, but the corrosion rate of Ni-P coating after HT and PA is different from that of 20# steel. The corrosion rate of Ni-P coating after HT and PA is stable in the whole immersing period, and the increase amplitude is

minimal with the extension of immersing time.

The Ni-P coating, as a functional coating, protects 20# steel and therefore has a lower corrosion rate than 20# steel when immersed in simulated soil solution for the same time. However, the corrosion rate of Ni-P coating is also significantly accelerated at the later stage of immersing in simulated soil solution. The corrosion resistance of Ni-P coating has been reported by some researchers [14-18]. Heat treatment can reduce the defects in Ni-P coating and eliminate the internal stress, which is beneficial to improve the pitting resistance of Ni-P coating. The effect of heat treatment on the structure of Ni-P coating is also investigated by some scholars who find that the Ni_2P and Ni_3P structures can be obtained after heat treatment [19-21]. Therefore, the corrosion rate of the HT Ni-P coating is lower than that of Ni-P coating. During potassium dichromate passivation, a passivation film is formed to cover the surface of Ni-P coating, which acts as a physical barrier to prevent corrosive ions. In addition, with the extension of immersing time, a dense corrosion products film is gradually formed on the Ni-P coating after HT and PA, which can delay the corrosion development for a long time. Therefore, the corrosion rate of the Ni-P coating after HT and PA in simulated soil solution remains low for a long time, which is about 0.12 $g/(cm^2 \cdot d)$.
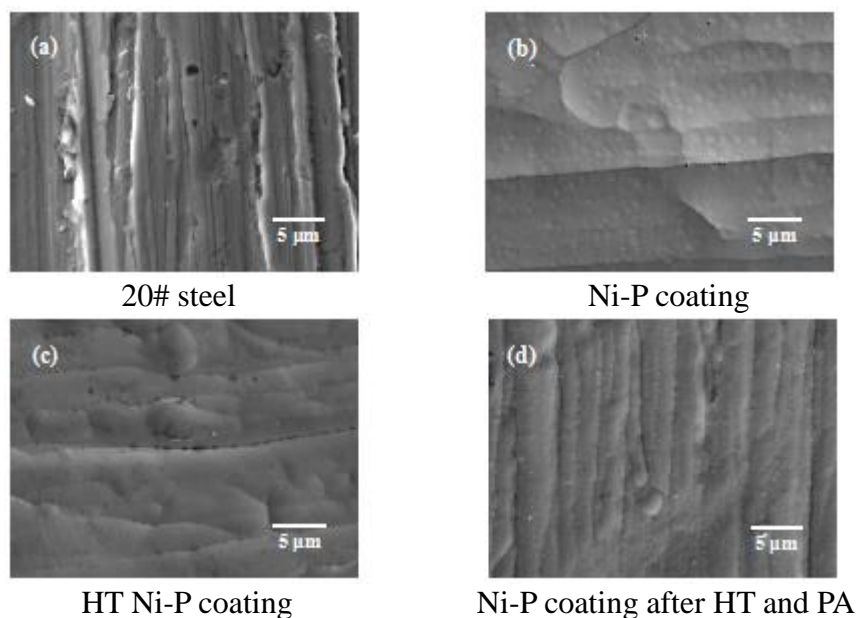

Figure 1. Corrosion rate of different samples after immersing in simulated soil solution for different time; (heat treatment of Ni-P coating in the muffle furnace at 400 °C for 1 hour is defined as HT Ni-P coating; after heat treatment, the Ni-P coating is immersed in the passivation solution with potassium dichromate for 10 minutes at 60 ℃ to carry out the passivation is defined as Ni-P coating after HT and PA)

*3.2 Surface morphology and corrosion morphology analysis*

Figure 2 shows the surface morphology of different samples. As shown in Figure 2(a), the surface of 20# steel is flat except for strip wear marks and different pits. As shown in Figure 2(b), the surface of Ni-P coating is flat and compact except for some micro-pores and the grain boundaries are not clear, which indicates that the Ni-P coating prepared in this paper has an amorphous structure, which is consistent with the experimental results of scholars [22-25]. As can be seen in Figure 2(c), the HT Ni-P coating still maintains amorphous structure, and the surface flatness and compactness do not

change significantly compared with Ni-P coating, but there are few micro-pores. The reason is that heat treatment reduces the defects in Ni-P coating. As can be seen in Figure 2(d), there are almost no micro-pores on the surface of the Ni-P coating after HT and PA, which still maintains the amorphous structure and is generally flat and compact. But its morphology feature is different from that of Ni-P coating. During the process of potassium dichromate passivation, a passivation film is generated to cover the surface of Ni-P coating, which changes its surface morphology. In addition, the uniform coverage of the passivation film makes almost no micro-pores on the surface of Ni-P coating.

20# steel	Ni-P coating
HT Ni-P coating	Ni-P coating after HT and PA

Figure 2. Surface morphology of different samples; (accelerating voltage is 10 kV and working distance is 8.2 mm with magnification 10000 times)
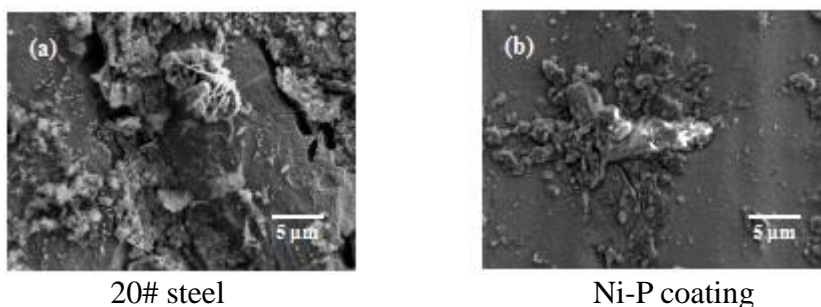
Figure 3 shows the corrosion morphology of different samples immersed in simulated soil solution for 7 days. As shown in Figure 3(a), many granular materials generate on the surface of 20# steel. However, the granular materials are closely combined and accumulated to form a dense corrosion products film, which could prevent corrosive ions. As shown in Figure 3(b), some granular materials generate on the surface of Ni-P coating, indicating that the corrosion degree is aggravated with the extension of immersing time in simulated soil solution. As shown in Figure 3(c) and Figure 3(d), a small amount of granular materials generate on the surface of the HT Ni-P coating and the Ni-P coating after HT and PA, which shows good corrosion resistance.

20# steel	Ni-P coating

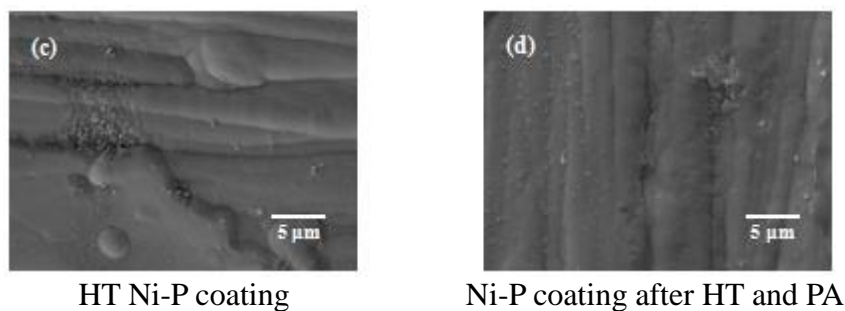HT Ni-P coating   Ni-P coating after HT and PA
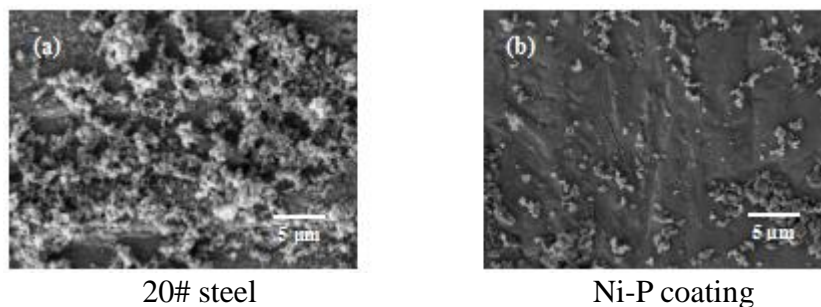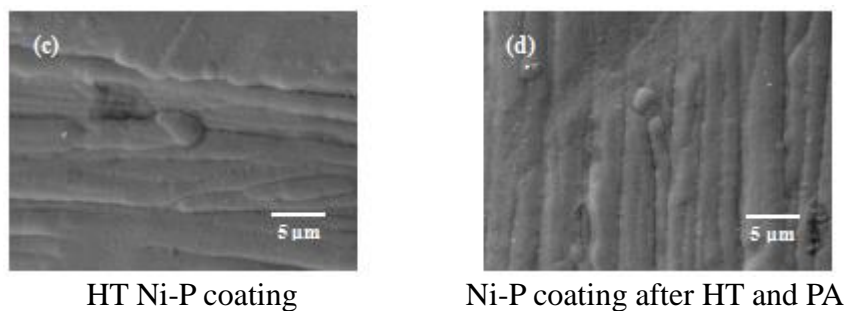
Figure 3. Corrosion morphology of different samples immersed in simulated soil solution for 7 days; (accelerating voltage is 10 kV and working distance is 8.2 mm with magnification 10000 times)

Figure 4 shows the corrosion morphology of different samples immersed in simulated soil solution for 16 days. As shown in Figure 4(a), the cluster particles appear on the surface of 20# steel and cracks are formed in some parts, which confirm that 20# steel is severely corroded in the later stage of immersing in simulated soil solution. As shown in Figure 4(b), the Ni-P coating also corrodes seriously immersed in simulated soil solution for 16 days. Although Ni-P coating has a relatively good corrosion resistance due to the amorphous structure, there are some micro-pores in Ni-P coating, and the corrosive ions in simulated soil solution will diffuse along the micro-pores to aggravate the corrosion degree. As shown in Figure 4(c), the corrosion degree of the HT Ni-P coating is reduced compared with that of Ni-P coating immersed in simulated soil solution for 16 days. The reason is that heat treatment can reduce the defects in Ni-P coating and improve the corrosion resistance of the coating, thus showing that the corrosion degree is lightened. As shown in Figure 4(d), the corrosion degree of the Ni-P coating after HT and PA is still the lightest after immersing in simulated soil solution for 16 days, and only some scattered granular materials generate on the surface without cracks. On the one hand, heat treatment can decrease the defects in Ni-P coating, which is conducive to improve the corrosion resistance of the coating. On the other hand, during the passivation process, a passivation film is formed to cover the surface of the coating, which acts as a physical barrier to prevent corrosive ions and reduce the corrosion tendency of the coating. Passivation treatment can effectively improve the corrosion resistance of metal alloys which is also reported in some literatures [26-28]. Therefore, the Ni-P coating after HT and PA can maintain good corrosion resistance in simulated soil solution for a long time.

20# steel   Ni-P coating

HT Ni-P coating   Ni-P coating after HT and PA

Figure 4. Corrosion morphology of different samples immersed in simulated soil solution for 16 days; (accelerating voltage is 10 kV and working distance is 8.2 mm with magnification 10000 times)

3.3 Potentiodynamic polarization curves analysis

(a) short-time immersing

(b) immersing for 7 days

(c) immersing for 16 days
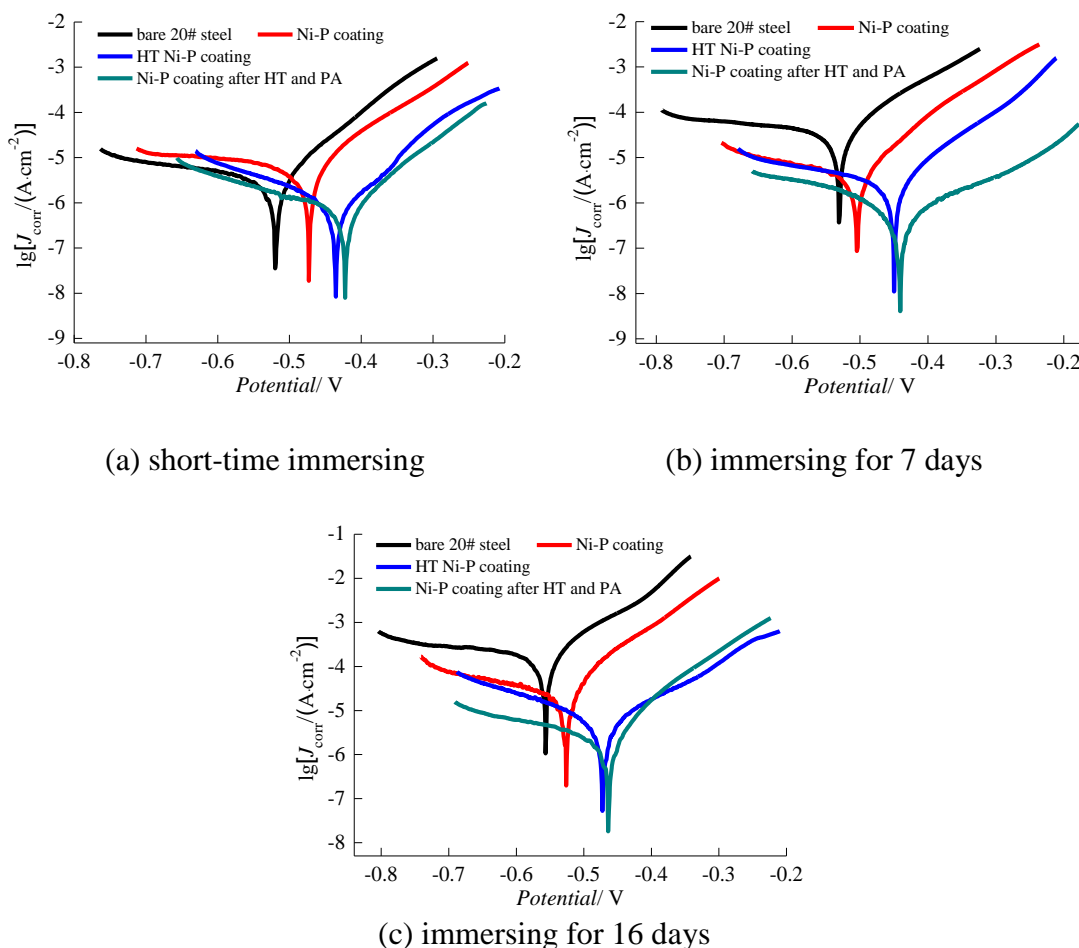
Figure 5. Potentiodynamic polarization curves of different samples immersed in simulated soil solution for different time; (the saturated calomel electrode, platinum sheet and different samples are used as reference electrode, auxiliary electrode and working electrodes, respectively; the scan rate of potentiodynamic polarization curve is 1 mV/s)

Figure 5 shows the potentiodynamic polarization curves of different samples immersed in

simulated soil solution for different time. Combined Figure 5(a), 5(b) and 5(c), it can be seen that the potentiodynamic polarization curves of 20# steel, Ni-P coating, HT Ni-P coating and the Ni-P coating after HT and PA do not have passivation zone in simulated soil solution.

According to the potentiodynamic polarization curves fitting results listed in Table 3, the corrosion potential of 20# steel, Ni-P coating, HT Ni-P coating and the Ni-P coating after HT and PA in simulated soil solution basically moves to more negative direction with the extension of immersing time. It can also be seen from Table 2 that the corrosion current density of 20# steel, Ni-P coating and HT Ni-P coating in simulated soil solution basically increases with the extension of immersing time, while the corrosion current density of the Ni-P coating after HT and PA increases slowly with the extension of immersing time. For example, the corrosion current density of 20# steel increases from 5.91×10^{-5} A/cm^2 to 2.06×10^{-4} A/cm^2 when the immersing time in simulated soil solution is extended from 7 to 16 days. However, the corrosion current density of the Ni-P coating after HT and PA increases slowly from 1.78×10^{-6} A/cm^2 to 2.49×10^{-6} A/cm^2. The research shows that the higher the corrosion current density, the faster the corrosion rate of the material in the corrosion medium [29-30]. The corrosion current density tends to be stable, indicating that the corrosion process of the material is effectively suppressed. Potentiodynamic polarization curves, corrosion rate and corrosion morphology analysis results show that the Ni-P coating after HT and PA has amorphous structure and the best corrosion resistance which can provide excellent protection effect for 20# steel in simulated soil solution.

Table 3. Corrosion potential and corrosion current density of different samples immersed in simulated soil solution for different time

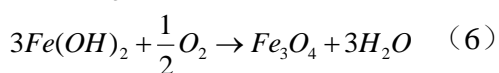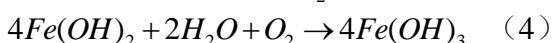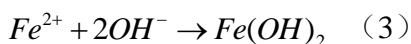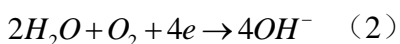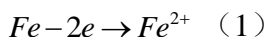| Different samples	Corrosion potential/ V			Corrosion current density/ (A·cm^{-2})		
	short-time immersing	immersed for 7 days	immersed for 16 days	short-time immersing	immersed for 7 days	immersed for 16 days
20# steel	-0.519	-0.530	-0.556	3.12×10^{-5}	5.91×10^{-5}	2.06×10^{-4}
Ni-P coating	-0.472	-0.504	-0.526	5.03×10^{-6}	8.51×10^{-6}	2.93×10^{-5}
HT Ni-P coating	-0.436	-0.450	-0.471	1.74×10^{-6}	3.21×10^{-6}	8.02×10^{-6}
Ni-P coating after HT and PA	-0.422	-0.441	-0.460	9.64×10^{-7}	1.78×10^{-6}	2.49×10^{-6}

3.4 Corrosion products analysis

Table 4 shows the corrosion products on the surface of 20# steel and the Ni-P coating after HT and PA immersed in simulated soil solution for different time. According to the composition, the corrosion products generate on 20# steel are mainly carbon oxide, FeOOH and Fe_3O_4, and the reactions are shown by Equation (1)~(6) during the corrosion process [31-32]. Carbon oxide is oxygen dissolved in simulated soil solution combined with carbide on the surface of 20# steel. During the corrosion process, the anodic reaction is Fe dissolution reaction to form Fe^{2+}, and the cathodic reaction is oxygen absorption reaction to form OH^-, and then $Fe(OH)_2$ and $Fe(OH)_3$ are formed. Since $Fe(OH)_2$ and $Fe(OH)_3$ are extremely unstable, the reaction continues to form Fe_3O_4.

According to the composition, the corrosion products on the surface of the Ni-P coating after HT and PA are carbon oxides, $Ni(OH)_2$ and a small amount of FeOOH and Fe_3O_4. During the corrosion process, the dissolution reaction of Ni occurs to generate Ni^{2+}. At the same time, the oxygen absorption reaction generates OH^-, and finally generates $Ni(OH)_2$.

In the later stage of corrosion in simulated soil solution, local damage occurred due to the aggravated corrosion of the coating. Corrosive ions penetrate the damaged area and contact the 20# steel, leading to a certain degree of corrosion and a small amount of FeOOH and Fe_3O_4 is generated. In comparison, the corrosion products on the Ni-P coating after HT and PA immersed in simulated soil solution for 16 days contain lower mass fraction of C, O and Fe elements. It is further confirmed that the Ni-P coating after HT and PA has the best corrosion resistance and it can provide excellent protection for 20# steel in simulated soil solution.

Table 4. Composition of corrosion products on the surface of 20# steel and the Ni-P coating after HT and PA (working voltage is 10 kV, surface scanning mode)

Element and composition		Different samples	
		20# steel	Ni-P coating after HT and PA
C	immersed for 7 days	18.46%	9.15%
	immersed for 16 days	13.32%	9.11%
O	immersed for 7 days	37.15%	30.29%
	immersed for 16 days	40.28%	26.68%
Fe	immersed for 7 days	44.39%	0.36%
	immersed for 16 days	46.40%	0.79%
Ni	immersed for 7 days	—	60.20%
	immersed for 16 days	—	63.42%

$$Fe - 2e \rightarrow Fe^{2+} \quad （1）$$
$$2H_2O + O_2 + 4e \rightarrow 4OH^- \quad （2）$$
$$Fe^{2+} + 2OH^- \rightarrow Fe(OH)_2 \quad （3）$$
$$4Fe(OH)_2 + 2H_2O + O_2 \rightarrow 4Fe(OH)_3 \quad （4）$$
$$Fe(OH)_3 \rightarrow FeOOH + H_2O \quad （5）$$
$$3Fe(OH)_2 + \frac{1}{2}O_2 \rightarrow Fe_3O_4 + 3H_2O \quad （6）$$

4. CONCLUSIONS

(1) With the immersing time in simulated soil solution extends to 16 days, the corrosion rate and corrosion current density of 20# steel show a trend of slowly increasing at first and then significantly increasing, while the corrosion rate and corrosion current density of the Ni-P coating after heat treatment and passivation show a trend of slowly increasing. The Ni-P coating after heat treatment

and passivation still maintains a low corrosion rate of 0.12 g/(cm^2·d) and corrosion current density of 2.49×10^{-6} A/cm^2 after immersing in simulated soil solution for a long time, indicating excellent corrosion resistance.

(2) Electroless Ni-P coating has an amorphous structure and its corrosion resistance is relatively good. Heat treatment can reduce the defects in the coating to reduce corrosion tendency and corrosion rate. Moreover, the passivation is carried out to generate a passivation film covering the surface of the coating to play a physical barrier role, and further delay the development of corrosion process. The Ni-P coating after heat and passivation treatment presents an excellent corrosion resistance performance which is beneficial to protect 20# steel in simulated soil solution.

References

1. L. X. Wei, Y. Ge, Q. H. Gao, C. Wang, X. Yu and L. Zhang, *J. Electroanal. Chem.*, 921 (2022) 116714.
2. J. B. Xue, J. L. Gao, Q. Q. Shen, Q. Li, X. G. Liu, H. S. Jia and Y. C. Wu, *Surf. Coat. Technol.*, 385 (2020) 125445.
3. T. Z. Xu, S. Zhang, Z. Y. Wang, C. H. Zhang, D. X. Zhang, M. Wang and C. L. Wu, *Eng. Fail. Anal.*, 141 (2022) 106698.
4. Y. W. Dong, G. Z. Kang, Y. J. Liu and H. Jiang, *Mater. Charact.*, 83 (2013) 1.
5. O. Singh, H. K. Malik, R. P. Dahiya and P. K. Kulriya, *J. Alloys Compd.*, 710 (2017) 253.
6. D. Wang, T. J. Li, F. Xie, Y. Wang and H. Q. Wang, *Constr. Build. Mater.*, 350 (2022) 128897.
7. R. S. Zheng, X. Y. Zhao, L. L. Dong, G. Liu, Y. Huang and Y. Z. Xu, *Eng. Fail. Anal.*, 138 (2022) 106333.
8. R. Zhou, X. T. Gu, S. B. Bi and J. Wang, *Eng. Fail. Anal.*, 136 (2022) 106203.
9. X. Z. Li, Z. D. Liu, H. C. Li, Y. T. Wang and B. Li, *Surf. Coat. Technol.*, 232 (2013) 627.
10. N. M. Lin, P. Zhou, J. J. Zou, F. Q. Xie and B. Tang, *J. Wuhan Univ. Technol. Mater. Sci. Ed.*, 30 (2015) 622.
11. W. Tian, W. H. Yu, N. M. Lin and J. J. Zou, *Int. J. Electrochem. Sci.*, 10 (2015) 6057.
12. E. M. Sherif, M. M. E. Rayes and H. S. Abdo, *Coatings*, 10 (2020) 275.
13. C. H. Wang, Z. Farhat, G. Jarjoura, M. K. Hassan and A. M. Abdullah, *Wear*, 376 (2017) 1630.
14. M. H. Sliem, K. Shahzad, V. N. Sivaprasad, R. A. Shakoor, A. M. Abdullah, O. Fayyaz, R. Kahraman and M. A. Umer, *Surf. Coat. Technol.*, 403 (2020) 126340.
15. E. M. Fayyad, M. K. Hassan, K. Rasool, K. A. Mahmoud, M. A. Mohamed, G. Jarjoura, Z. Farhat and A. M. Abdullah, *Surf. Coat. Technol.*, 369 (2019) 323.
16. A. P. Meshram, M. K. P. Kumar and C. Srivastava, *Diamond Relat. Mater.*, 105 (2020) 107795.
17. D. F. Carrillo, A. Bermudez, M. A. Gomez, A. A. Zuleta, J. G. Castano and S. Mischler, *Surf. Interfaces*, 21 (2020) 100733.
18. W. P. Wu, X. Wang, D. K. Xie, Y. Zhang and J. W. Liu, *Eng. Fail. Anal.*, 111 (2020) 104497.
19. D. Ahmadkhaniha, F. Eriksson, P. Leisner and C. Zanella, *J. Alloys Compd.,* 769 (2018) 1080.
20. A. Z. Karathanasis, E. A. Pavlatou and N. Spyrellis, *Electrochim. Acta,* 54 (2009) 2563.
21. I. Apachitei, F. D. Tichelaar, J. Duszczyk and L. Katgerman, *Surf. Coat. Technol.,* 149 (2002) 263.
22. G. M. Song, Y. Wu, Q. Xu and G. Liu, *J. Power Sources*, 195 (2010) 3913.
23. 20. C. A. Vlaic, M. Kurniawan, R. Peipmann, C. C. Lalau, M. Stich, U. Schmidt and A. Bund, *Surf. Coat. Technol.*, 386 (2020) 125470.
24. B. Bozzini, P. L. Cavallotti, J. P. Celis and A. Fanigliulo, *Corros. Sci.*, 45 (2003) 1161.
25. Y. Xu, X. M. Ge, Y. J. Tong, H. L. Xie, T. Q. Xiao and J. Z. Jiang, *Electrochem. Commun.*, 12 (2010) 442.

26. L. T. Wu, Z. H. Zhou, K. C. Zhang, X. Zhang and G. Y. Wang, *J. Non-Cryst. Solids,* 597 (2022) 121892.
27. R. Wang, D. T. Wang, H. M. Nagaumi, Z. B. Wu, X. Z. Li and H. T. Zhang, *Corros. Sci.,* 205 (2022) 110468.
28. D. S. Hou, K. X. Zhang, F. Hong, S. R. Wu, Z. Wang, M. M. Li and M. H. Wang, *Appl. Surf. Sci.,* 582 (2022) 152408.
29. Z. Shao, M. Nishimoto, L. Muto and Y. Sugawara, *Corros. Sci.,* 192 (2021) 109834.
30. L. J. Chen and R. K. L. Su, *Constr. Build. Mater.,* 267 (2021) 121003.
31. Y. Q. Liu and J. J. Shi, *Corros. Sci.,* 205 (2022) 110451.
32. L. B. Jin, X. W. Zhang, X. Y. Liang, Z. Q. Wang and Q. Wu, *Ocean Eng.,* 260 (2022) 111759.